Article:
Schremb, M, Campbell, JM, Christenson, HK et al. (2017) Ice Layer Spreading along a Solid Substrate during Solidification of Supercooled Water: Experiments and Modeling. Langmuir, 33 (19). pp. 4870-4877. ISSN: 0743-7463

https://doi.org/10.1021/acs.langmuir.7b00930

Ice Layer Spreading along a Solid Substrate during Solidification of Supercooled Water: Experiments and Modeling

Markus Schremb,*,† James M. Campbell,‡ Hugo K. Christenson,‡ and Cameron Tropea†

†*Institute of Fluid Mechanics and Aerodynamics, Technische Universität Darmstadt, Darmstadt, Germany*

‡*School of Physics and Astronomy, University of Leeds, Leeds, United Kingdom*

E-mail: schremb@sla.tu-darmstadt.de

Abstract

The thermal influence of a solid wall on the solidification of a sessile supercooled water drop is experimentally investigated. The velocity of the initial ice layer propagating along the solid substrate prior to dendritic solidification is determined from videos captured using a high-speed video system. Experiments are performed for varying substrate materials and liquid supercooling. In contrast to recent studies at moderate supercooling, in the case of metallic substrates only a weak influence of the substrate's thermal properties on the ice layer velocity is observed. Using the analytical solution of the two-phase Stefan problem, a semi-empirical model for the ice layer velocity is developed. The experimental data are well described for all supercooling levels in the entire diffusion limited solidification regime. For higher supercooling, the model overestimates the freezing velocity due to kinetic effects during molecular attachment at

the solid-liquid interface, which are not accounted for in the model. The experimental findings of the present work offer a new perspective on the design of anti-icing systems.

Introduction

Icing of solid surfaces is an ever-present safety issue in many engineering systems. It poses a severe hazard for aircraft[1–3] and ships,[4] but is also a frequent problem for road traffic,[5] wind turbines[6] and power supply systems.[7–10] Ice accretion may result from the impact of warm water droplets on surfaces at subfreezing temperatures (road icing), the impact of ice crystals on warm surfaces (jet engine icing) or from the impact of supercooled liquid drops on cold surfaces (airframe icing). In all cases, a thorough understanding of the mechanisms leading to ice accretion is of fundamental importance for the reduction or prevention of icing. Depending on the particular icing mechanism, the physical processes taking place during ice accretion are very different.

Ice accretion due to the impact of supercooled water drops depends on several physical processes taking place in parallel or succession. It starts with the impact of a liquid drop,[11–14] is followed by nucleation of the moving liquid[13–15] and ends up with the solidification of the liquid in successive stages, ultimately determining the actual shape of the drop.[15–19]

The dynamics during drop impact depend in particular on the impact parameters, such as the impact velocity and drop diameter. Together with the liquid properties, which may strongly depend on temperature, the impact parameters determine the maximum drop spreading, which represents the maximum iced area after a single drop impact. Nucleation mainly depends on the liquid temperature,[20,21] but may also be affected by the surface properties,[20] shear flow during impact,[22] temperature gradients within the liquid as a consequence of non-isothermal drop impact,[23] or other mechanisms, such as gas bubble entrainment during impact.[14] In contrast to the aforementioned processes, the speed of dendritic solidification of the bulk of a supercooled liquid just depends on one parameter: the liquid

supercooling.[19,24–27] However, in the case of solidification of a supercooled liquid in contact with a solid wall, the solidification process is further influenced by the material properties of the solid material.[18]

Similar to the multitude of mechanisms taking place during ice accretion, also the number of approaches for the reduction and prevention of icing are manifold.[28] By utilizing superhydrophobic surfaces, these approaches are often based on a general increase of the freezing delay,[29–31] a decrease of wettability resulting in drop repulsion before nucleation,[32,33] reduction of the ice adhesion strength to the surface,[34] or an increase of the drop mobility on the surface to promote drop shedding.[35]

All of these approaches target processes before solidification, i.e. drop impact and nucleation, and time always plays an important role. Kong and Liu[18] observed a strong dependence of the freezing velocity along a solid wall on the substrate's material properties. However, although the freezing velocity significantly influences the time available for drop repulsion or shedding, to the authors' knowledge, no anti-icing approach takes into account the freezing process itself as a tunable mechanism during surface icing.

Therefore, in the present study, an experimental facility, first introduced by Schremb and Tropea,[19] is used to investigate the thermal influence of a solid substrate on the solidification of a supercooled water drop. The facility enables two-dimensional examination of the solidification process with a high-speed video system. Material properties are varied and their influence on the solidification velocity along the substrate is outlined. Based on the two-phase Stefan problem, a semi-empirical model is developed, allowing the prediction of the ice layer speed depending on the initial liquid supercooling and the material properties of the solid substrate. By demonstrating a strong influence of the substrate material properties on the freezing process, the present study may serve as a building block for the future design of anti-icing surfaces.

Experimental Method

The experimental method and first results including snapshots and videos of the overall solidification process of a supercooled water drop at a solid wall have been introduced in Schremb and Tropea.[19] Therefore, only a brief overview of the basic features is given here. The setup consists of a cooling system and an optical observation system. The main part of the cooling system is a vertically oriented Hele-Shaw cell consisting of two side walls made of acrylic glass and an exchangable spacer at the base made of a variable smoothed material which provides a constant distance between the side walls. Both the acrylic glass sheets and the spacer are stacked and fixed in an aluminum base. A water drop (Milli-Q Type 1, electrical conductivity $\sigma \approx 5.5 * 10^{-6}$ S/m at 25 °C) is trapped between the side walls and is in direct contact with the spacer material as depicted in Fig. 1.

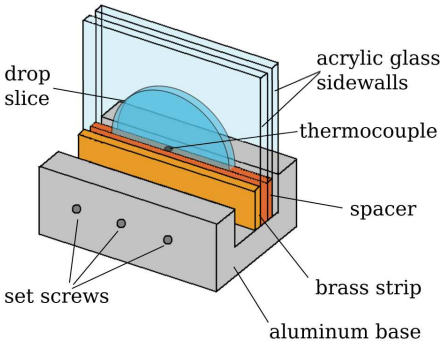

Figure 1: Schematic of the Hele-Shaw cell with an inserted drop.

The Hele-Shaw cell is placed on a cooling plate in a closed styrofoam chamber. Gaseous nitrogen within the chamber prevents the build-up of frost and condensate on the cold surfaces. A double glassed side window provides optical access to the styrofoam chamber and the Hele-Shaw cell.

A thermocouple with a diameter of 0.5 mm is immersed into the spacer substrate of the Hele-Shaw cell. While the temperature has been measured within the spacer in Schremb and Tropea,[19] in the present study, the thermocouple does not end in the spacer, but at its surface, as shown in Fig. 2. Therefore, the liquid temperature is measured at the bottom of

the drop and the measurement is uninfluenced by thermal conduction within the spacer. No significant influence of the thermocouple on the nucleation process could be observed.

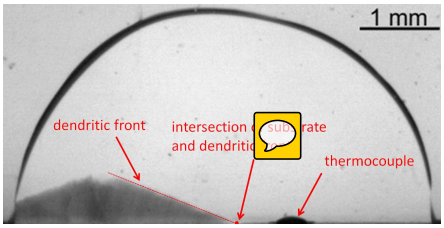

Figure 2: Two dimensional side view of the dendritic solidification of a water drop at approximately −15 °C entrapped in the Hele-Shaw cell. The drop temperature is measured with a thermocouple ending at the bottom of the drop.

A high-speed video camera (*Photron* MC 2.1), LED illumination and a diffusor screen are used to capture the solidification process by means of backlight shadowgraphy imaging. Videos are recorded with a frame rate and optical resolution of 2000 fps and approx. 13 μm/pixel, respectively.

Water drops with volumes ranging from 1.5 μl to 10 μl are used for the experiments. The liquid temperature ranges from −1.4 °C to −19.3 °C. Schremb and Tropea[19] only used a copper substrate to examine the freezing process along a solid wall. In the present study, we expand these results by choosing substrate materials with thermal properties varying in a wide range as summarized in Table 1.

Table 1: Density ρ, heat capacity c_p, thermal conductivity k, thermal diffusivity a and thermal effusivity $\epsilon = \sqrt{\rho c_\mathrm{p} k}$ of ice, water and the substrates used in the present study.[36,37]

	ρ $\left[\frac{\mathrm{kg}}{\mathrm{m}^3}\right]$	c_p $\left[\frac{\mathrm{J}}{\mathrm{kgK}}\right]$	k $\left[\frac{\mathrm{W}}{\mathrm{mK}}\right]$	α $\left[10^{-6}\frac{\mathrm{m}^2}{\mathrm{s}}\right]$	ϵ $\left[\frac{\mathrm{Ws}^{0.5}}{\mathrm{m}^2\mathrm{K}}\right]$
Copper	8954	384	398	115.75	37000
Aluminum	2707	905	237	96.74	24100
Brass	8522	385	109	33.22	18900
Stainless steel	8000	400	14	4.38	6700
Ice (0 °C)	917	2100	2.215	1.15	2065
Water (0 °C)	1000	4219	0.562	0.133	1540
Acrylic glass	1180	1260	0.19	0.128	531

At the beginning of an experiment, a drop at room temperature is placed into the Hele-Shaw cell, which is subsequently placed onto the cooling plate precooled to 0°C. Then the cooling plate and the Hele-Shaw cell containing the water drop are simultaneously cooled down at a moderate cooling rate of 0.2 K/s. For large supercooling, freezing automatically starts due to heterogeneous nucleation at the liquid-solid interface. To allow observation of the freezing process also for moderate supercoolings, in these cases solidification is triggered with a thin piece of acrylic glass brought into contact with the supercooled drop at the water-air-substrate contact line.

Solidification of the liquid results in a fast warming-up of the drop. Therefore, the drop supercooling is determined from the lowest temperature value before the sudden temperature increase.

Results and Discussion

As described by Kong and Liu,[18] and Schremb and Tropea,[19] solidification of supercooled water in the vicinity of a solid wall comprises three consecutive phases:

1. Heterogeneous nucleation at the wall is followed by the tangential growth of a thin ice layer spreading over the substrate-water interface with a constant speed, which depends on supercooling. As already reported in Schremb and Tropea,[19] nucleation occurs at a random position of the wetted substrate and is not preferential at the three-phase contact line. For supercoolings up to $\Delta T = 7\,\mathrm{K}$ the velocity of the initial ice layer strongly depends on the material properties of the solid substrate.[18] However, Kong and Liu,[18] and Schremb and Tropea[19] suggested that the solidification velocity is only weakly influenced by the substrate material for larger supercooling.

2. For large supercoolings, the surface of the initial ice layer becomes unstable at a certain position behind the tip of the ice layer resulting in the growth of single dendrites or a front of numerous dendrites into the bulk liquid. The supercooling threshold for

unstable growth was found as $\Delta T = 2.6\,\mathrm{K}$ in Kong and Liu[18] and as $\Delta T = 4.7\,\mathrm{K}$ in Schremb and Tropea.[19] For supercoolings below this threshold, only planar growth of the thin ice layer has been observed. It has been shown that also the position of the first instability behind the tip and the morphology of dendritic solidification depends on supercooling as shown in Table 2.[19] The higher the supercooling, the closer to the ice layer tip is the position of the first instability of the ice layer surface. While single dendrites are observed for smaller supercooling, the dendrite density increases with increasing supercooling, resulting in a dense front of dendrites for large supercooling. Only small mutual influence of the dendrites has been observed. Therefore, all dendrites propagate at approximately the same speed as a single dendrite.[19] At the end of the second phase, only a portion of the initially supercooled drop is frozen and a lattice of dendritic ice fills out the entire drop. The latent heat released during solidification has warmed up the water-ice mixture to thermodynamic equilibrium at the melting temperature.

3. A further removal of heat results in stable freezing of the remaining water. The stable freezing front in this phase moves in the opposite direction of the applied heat flux.

As shown above, several processes involving different physical mechanisms take place during the solidification of a supercooled drop. The entire process is highly complex and therefore it is convenient to split it up and to describe the different processes separately. Accordingly, the focus of the present study is only on the first phase of solidification, i.e. the rapid spreading of an ice layer over the substrate surface.

Experimental Results

Figure 3 shows the experimentally measured ice layer velocities for varying degrees of supercooling and substrate materials. For comparison, experimental data of Shibkov et al.[27] for the velocity of a single dendrite growing freely in supercooled water is also shown. In

Table 2: Freezing morphologies of the first phase of supercooled freezing depending on the liquid supercooling. The tip of the initial ice layer is at the left side of each photograph and inserted vertical lines indicate the position of first visible instabilities. (From Schremb and Tropea.[19])

Description	Supercooling [K]	Detail
Planar	0...4.7	
Late dendrites	4.7...7.2	
Single dendrites	7.2...9.9	
Inhomogeneous front	9.9...12.0	
Homogeneous front	12.0...	

contrast to the solidification at the metallic surfaces, in the case of the acrylic glass substrate no explicit growth of a thin ice layer has been observed. Therefore, the movement of the intersection point of the dendritic front and the substrate surface (see Fig. 2) has been assumed to be comparable to the ice layer propagation. The horizontal velocity of this point is shown in Fig. 3. The solidification velocity on the acrylic glass substrate is very similar to the velocity of a single dendrite. Thus, the acrylic glass substrate acts as an adiabatic wall and does not thermally influence the solidification process in the near wall region.

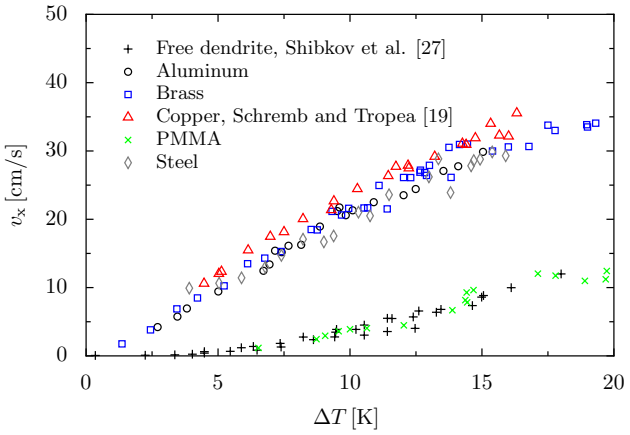

Figure 3: Layer velocity as a function of supercooling for varying substrate materials. Experimental data of Shibkov et al.[27] for the velocity of a single dendrite growing freely in supercooled water is also shown.

However, as already observed by Kong and Liu,[18] and Schremb and Tropea,[19] the ice

layer velocity is drastically enhanced by the presence of a metallic substrate in comparison to the velocity of a single dendrite. Furthermore, a strong dependence of the ice layer velocity on the substrate material has been observed for supercoolings up to $\Delta T = 7\,\mathrm{K}$ by Kong and Liu.[18] However, as shown in Fig. 3, in the case of metallic substrates the substrate material only weakly influences the ice layer propagation velocity for larger supercooling.

Theoretical Modeling of Ice Layer Spreading

The solidification of supercooled water at a solid substrate has been theoretically described by Kong and Liu.[18] They modeled the propagation of the initial ice layer by considering heat conduction in the supercooled liquid and the neighboring solid substrate. The ice layer velocity was described using a parabolic coordinate system, a moving reference frame and a length parameter to characterize the ice layer thickness.

In the present study we propose a simple model based on the analytic solution of the two-phase Stefan problem. For its derivation, let us first have a look at the one-dimensional case of ice layer growth, where solidification starts at the same time at each point of a surface.

Consider a semi-infinite slab, $0 \leq y < \infty$, of supercooled water initially at $T_\mathrm{l} < T_\mathrm{m}$, where T_m is the liquid melting temperature. At time $t = 0$, the temperature T_c is imposed at the boundary $y = 0$, and solidification starts, resulting in a planar freezing front moving parallel to the substrate surface into the supercooled liquid $y > 0$. The resulting temperature profiles in the liquid phase and the growing solid layer are qualitatively shown in Fig. 4. In the case

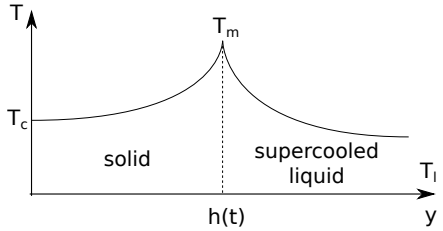

Figure 4: Resulting temperature profiles in the solid and liquid phase during planar freezing of a supercooled liquid.

of $T_\mathrm{l} < T_\mathrm{m}$ and $T_\mathrm{c} < T_\mathrm{m}$, the latent heat of fusion is released in both the liquid and the

solid phase, and the solidification process can be described as a two-phase Stefan problem.[38] Therefore, the temporal evolution of the ice layer thickness is

$$h(t) = 2\lambda\sqrt{\alpha_{\mathrm{s}} t}, \tag{1}$$

where α_{s} is the thermal diffusivity of ice and the parameter λ is the root of the transcendental equation

$$\frac{\mathrm{St_c}}{\lambda\sqrt{\pi}\exp(\lambda^2)\,\mathrm{erf}(\lambda)} + \frac{\mathrm{St_l}}{\nu\lambda\sqrt{\pi}\exp((\nu\lambda)^2)\,\mathrm{erfc}(\nu\lambda)} = 1. \tag{2}$$

The Stefan numbers are defined as

$$\mathrm{St_c} = \frac{c_{\mathrm{s}}(T_{\mathrm{m}} - T_{\mathrm{c}})}{L} \qquad \text{and} \qquad \mathrm{St_l} = \frac{c_{\mathrm{l}}(T_{\mathrm{m}} - T_{\mathrm{l}})}{L}, \tag{3}$$

where L is the latent heat of fusion, and c_{s} and c_{l} are the heat capacities of ice and water, respectively. The parameter ν in Eq. 2 is the square root of the ratio of the thermal diffusivities of ice and water

$$\nu = \sqrt{\frac{\alpha_{\mathrm{s}}}{\alpha_{\mathrm{l}}}}. \tag{4}$$

In reality, solidification does not start at the same time over the entire substrate surface, but only at a single nucleation site on the solid surface. Nucleation at time $t = 0$ and position $\vec{x} = 0$ is followed by the radial spreading of a thin ice layer over the substrate with a constant velocity v_{x}.[18,19] Solidification at an arbitrary point $\vec{x}$ on the surface starts at time

$$t = |\vec{x}|/v_{\mathrm{x}}. \tag{5}$$

Since the spreading velocity v_{x} is constant in time and space, it is sufficient and convenient to reduce the problem to two dimensions and to examine the ice layer growth in a plane, normal to the solid substrate and normal to the contact line between the ice, the surrounding water and the substrate, resulting in a cross-sectional view of the ice layer as schematically

shown in Fig. 5.

Solidification at the tip of the ice layer is determined by two-dimensional heat conduction in the supercooled liquid, the ice layer and the neighboring substrate. However, far behind the tip of the ice layer where $\mathrm{d}h/\mathrm{d}x << 1$, the movement of the ice-water interface is dominated by the vertical velocity v_{y}.[18]

Consider a coordinate system moving with the spreading ice layer and with its origin at the tip of the ice layer. In this moving reference frame, the ice layer thickness far behind the tip can be estimated from Eq. 1 and 5 as

$$h = 2\lambda\sqrt{\alpha_s \frac{x}{v_{\mathrm{x}}}}. \tag{6}$$

The underlying physical mechanisms of the ice layer growth are similar to those during the growth of a single dendrite. Therefore, it is reasonable to assume the temperature profile around the ice layer and the ice layer itself to be of parabolic shape.[18,24] Using this assumption, a second relation for the growing ice layer is obtained as

$$h = \sqrt{2Rx}, \tag{7}$$

where R is the tip radius of the ice layer, as shown in Fig. 5.

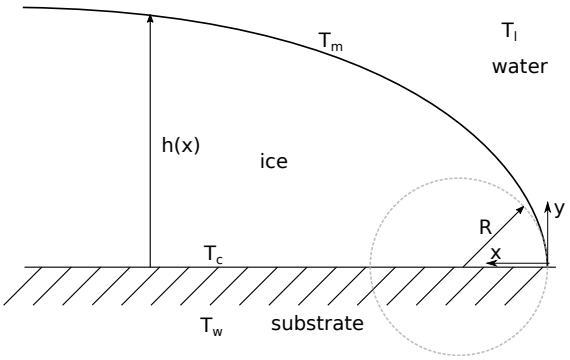

Figure 5: Cross-sectional view of the modeled ice layer.

Equating Eq. 6 and 7 yields the horizontal velocity of the ice layer

$$v_{\mathrm{x}} = \frac{2\lambda^2 \alpha_{\mathrm{s}}}{R} \tag{8}$$

where λ is calculated from Eq. 2.

In the case of an infinite thermal conductivity of the substrate, the characteristic temperature of the substrate surface far behind the tip, T_{c}, would be equal to the initial substrate temperature T_{w}. However, in the case of an adiabatic substrate, the surface temperature would be $T_{\mathrm{c}} = T_{\mathrm{m}}$ and the solidification process would not be affected by the presence of the substrate, as indicated above for acrylic glass as a low-conductivity substrate (Fig. 3). For a finitely conductive substrate, $T_{\mathrm{w}} \leq T_{\mathrm{c}} \leq T_{\mathrm{m}}$. From analogy with two semi-infinite solid slabs suddenly brought into contact with each other,[39] we estimate the surface temperature T_{c} at a position far behind the ice layer tip to be

$$T_{\mathrm{c}} = \frac{\epsilon_{\mathrm{s}} T_{\mathrm{m}} + \epsilon_{\mathrm{w}} T_{\mathrm{w}}}{\epsilon_{\mathrm{s}} + \epsilon_{\mathrm{w}}}. \tag{9}$$

The calculation of the ice layer speed for a given supercooling involves the estimation of the interface temperature using the initial temperatures and material properties in Eq. 9, the calculation of the parameter λ with Eq. 2 and finally, the calculation of the velocity with Eq. 8. The material properties for the calculations are all taken from Table 1, i.e. for a temperature of 0 °C. As seen from these relations, the substrate thermal properties are included into the theoretical model through Eq. 9. They implicitly influence the speed of the ice layer by affecting the temperature T_{c} of the substrate surface below the ice layer. The larger the thermal effusivity of the substrate material, the smaller is the warming up of the surface below the ice layer and consequently, the larger is the enhancement of the speed of solidification through the presence of the substrate. The temperature rise of the substrate, $T_{\mathrm{c}} - T_{\mathrm{w}}$, calculated with Eq. 9 for an initial substrate temperature $T_{\mathrm{w}} = -10\,^{\circ}\mathrm{C}$ and the examined substrate materials is examplarily shown in Table 3.

Table 3: Estimated temperature rise of the surface, $T_c - T_w$, due to solidification calculated with Eq. 9 for varying substrate materials and an initial substrate temperature $T_w = -10\,°C$.

substrate material	$T_c - T_w$ [K]
Copper	0.53
Aluminum	0.79
Brass	0.98
Stainless steel	2.36
Acrylic glass	7.95

The tip radius R, which is the only free parameter in the theoretical model, is obtained by a least-squares fit of Eq. 8 to the experimental data. As observed by Schremb and Tropea[19] for the solidification of supercooled water at a wall and by Shibkov et al.[27] for a single dendrite growing freely in supercooled water, above a certain supercooling the solidification process is affected by kinetic effects of molecular attachment at the ice-water interface. While the threshold for a single dendrite was found for supercoolings of $\Delta T > 4\,K$, this effect was observed for $\Delta T > 10\,K$ in the case of the solidification at a wall.[19] The present theoretical model only accounts for heat conduction and neglects kinetic effects involving a decreasing mobility of molecules for higher degrees of supercooling. Therefore, Eq. 8 is fitted to the experimental data only in the range $\Delta T \leq 10\,K$ to obtain the tip radius R for the so-called diffusion-limited growth regime. Since no ice layer growth has been observed for solidification on the acrylic glass substrate, the fitting is not applied to the data obtained with the acrylic glass substrate.

Figure 6 shows a comparison of the experimentally obtained layer velocities (circles) and the values theoretically calculated (lines) with the tip radii shown in Tab. 4 for all metallic substrate materials. The error of the temperature measurement is estimated as $\pm 0.3\,K$. Based on the frame rate and pixel-resolution of the high-speed video system, we estimate the relative error of the velocity measurement to be below $\pm 5\,\%$. As shown in the figure, the experimental data for $\Delta T \leq 10\,K$ is well described by the theoretical model for all

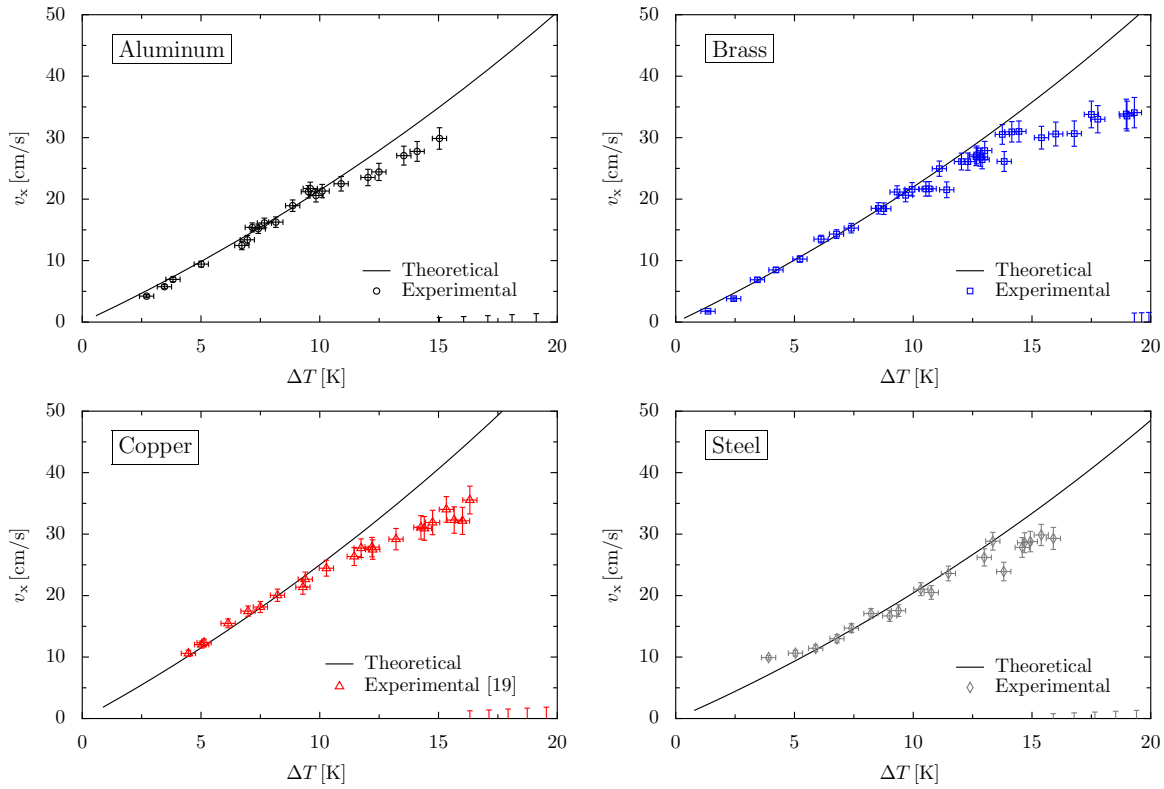

Figure 6: Ice layer velocity v_x depending on supercooling ΔT for different substrate materials and the tip radii summarized in Tab. 4. Comparison of experimental data (symbols) and the tip velocities theoretically modeled (lines).

substrate materials in the diffusion-limited growth regime. It is worth to note that the tip radius of the spreading ice layer is independent of the supercooling. However, in the case of a single dendrite growing freely in a supercooled melt, the tip radius depends on the liquid supercooling. It can be calculated using the marginal stability theory by Langer and Müller-Krumbhaar[40–42] which is based on a linear stability analysis for a planar freezing front.[43] In the range of supercooling examined in the present study, the tip radius of a free dendrite varies over two orders of magnitude between approximately 80 nm and 3 μm. According to the theory, a tip radius of a propagating ice layer of $R = 350$ nm corresponds to a single dendrite growing in a supercooled melt at approximately $-7.7\,^{\circ}$C. However, the reason for the constant tip radius in the case of a spreading ice layer is not clear and deserves further investigation.

As shown in Tab. 4, the tip radii for the different substrate materials vary by only 14 %

Table 4: Tip radius of the initial ice layer (Fig. 5) for varying substrate materials, obtained by fitting Eq. 8 to the experimental data for the supercooling range $\Delta T \leq 10\,\mathrm{K}$.

substrate material	tip radius [nm]
Copper	330
Aluminum	374
Brass	358
Stainless steel	329

and no correlation with any of the material properties shown in Tab. 1 can be observed. Therefore, we assume the tip radius to be a constant, which is not only independent of the supercooling, but also of the substrate material. Using the experimental data for all substrate materials (excluding acrylic glass) for fitting of Eq. 8, we obtain $R = 352\,\mathrm{nm}$ for the metallic materials. Figure 7 shows a direct comparison of the experimental and theoretical data for the ice layer velocity calculated with a constant tip radius $R = 352\,\mathrm{nm}$. The solid line represents perfect agreement between the calculated and the measured values. Even with the constraint of a substrate-independent tip radius, the theoretical model remains in very good agreement with the experimental data in the diffusion-limited growth regime. For layer velocities larger than $0.2\,\mathrm{m/s}$, an increasing deviation between the theoretical and experimental data is observable; the model overpredicts the layer velocity.

Figure 7 also shows a comparison for the data obtained on the acrylic glass substrate. The experimental data for acrylic glass is not used for the calculation of the tip radius R, and no distinct ice layer growth is observable on acrylic glass. Nevertheless, the agreement between the modeled growth velocity and the experimental values is very good.

Summary and Conclusions

The solidification of supercooled water close to a solid substrate has been experimentally investigated for temperatures down to $-19.3\,^{\circ}\mathrm{C}$. A Hele-Shaw cell combined with a high-speed

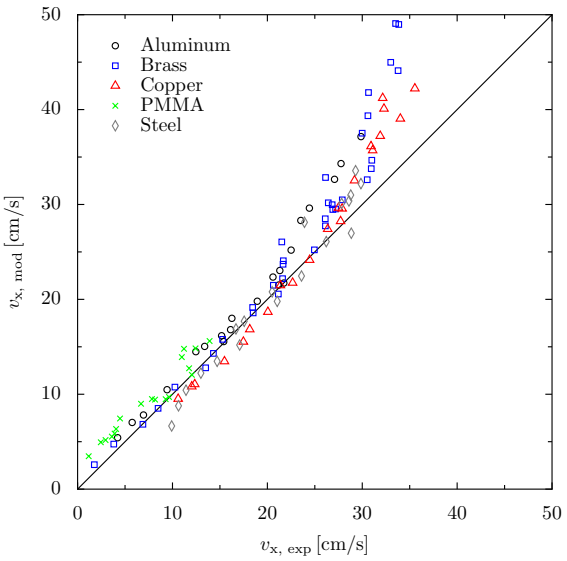

Figure 7: Comparison of the theoretically modeled and experimentally measured layer velocity for all substrate materials. A constant tip radius of $R = 352\,\mathrm{nm}$ was used for the calculation of v_x.

video system have been used to examine the influence of the substrate material properties on the spreading of a thin ice layer along the solid substrate prior to dendritic solidification of the bulk liquid.

The initial ice layer has only been observed in the case of metallic substrate materials. In the case of an acrylic glass substrate, the ice layer propagation has not been observed and the solidification process is not affected by the presence of the substrate. Therefore, the dendritic front close to the substrate propagates with the same velocity as in the bulk of a drop, which is comparable to that of a single dendrite. In the case of a metallic substrate, the solidification velocity is drastically increased at the substrate surface. For supercoolings up to 7 K, Kong and Liu[18] observed a strong influence of the substrate material properties on the velocity of the initial ice layer. However, we found only a slight dependence on the material properties for the of metallic substrates in the investigated temperature range.

The propagation of the initial ice layer in the diffusion-limited growth regime has been theoretically modeled. Based on the analytic solution of the two-phase Stefan problem, the model explicitly incorporates heat conduction in the supercooled liquid and in the growing

ice layer. Heat conduction in the solid wall, which is the origin of the increased velocity in the case of the metallic substrates, is implicitly accounted for by the estimation of the surface temperature below the ice layer. It is calculated using the equation for the contact temperature between two semi-infinite slabs of different temperature suddenly brought into contact. The only free parameter in the theoretical model is a length scale characterizing the tip radius of the propagating ice layer. It has been found by a least-squares fit of the theoretical model to the experimental data, and it has been shown that this parameter does not depend on the substrate material and is furthermore constant for the entire diffusion limited growth regime. The reasons for the constancy of the tip radius are not clear so far and therefore deserve further examination. However, the experimental data in the range of supercoolings $\Delta T \leq 10\,\mathrm{K}$ is well described by the semi-empirical model. For higher supercoolings, kinetic effects - which are not accounted for in the model - become important. These effects involve a decreasing speed of molecular attachment at the ice-water interface, which results in smaller velocities than predicted with the presented thermal model.

Most approaches for icing reduction and prevention only consider physical mechanisms prior to nucleation, i.e. when the liquid is still able to detach from the surface without freezing on it. These approaches comprise the reduction of the contact time and enhancement of drop rebound, or the increase of the freezing delay; and involve time as an important parameter. To the authors' knowledge, until now, no approach involves the processes taking place after nucleation, when there is no turning back from icing of the surface; although the possible potential is obvious: The freezing velocity at a solid substrate determines the time-scale of drop freezing, and hence the time available for processes such as drop rebound and flow-induced shedding of water from the surface. As shown in the present work, the freezing of supercooled water at a solid substrate may be slowed by a factor of approximately three by switching from a metallic substrate to an insulator such as acrylic glass. Therefore, the choice of the substrate material offers large potential for the optimization of icing prevention systems. It won't be possible to manufacture aircraft parts from a polymer like acrylic glass,

but suitable polymer coatings will probably have the same effect, as long as the coating is thicker than the characteristic length scale of the thermal boundary layer in the substrate.

Finally, the derived theoretical model provides a deeper insight into the influential mechanisms during ice accretion, and may be used to estimate the suitability of substrate materials for anti-icing applications by means of an accurate a-priori estimation of the surface freezing rate.

Acknowledgement

The authors gratefully acknowledge financial support from the Deutsche Forschungsgemeinschaft within the collaborative research project SFB-TRR 75 (TP-C3). Furthermore, HKC acknowledges support from the Leverhulme Trust (RPG-2014-306).

References

(1) Heinrich, A.; Ross, R.; Zumwalt, G.; Provorse, J.; Padmanabhan, V.; Thomson, J.; Riley, J. *Aircraft Icing Handbook: FAA Technical Report No. DOT/FAA/CT-88/8-1*; Technical report, 1991; Vol. 1,2,3.

(2) Cebeci, T.; Kafyeke, F. Aircraft Icing. *Annu. Rev. Fluid Mech.* **2003**, *35*, 11–21.

(3) Mason, J. G.; Strapp, J. W.; Chow, P. The Ice Particle Threat to Engines in Flight. 2006.

(4) Makkonen, L. Salinity and growth rate of ice formed by sea spray. *Cold Reg. Sci. Technol.* **1987**, *14*, 163–171.

(5) Symons, L.; Perry, A. Predicting road hazards caused by rain, freezing rain and wet surfaces and the role of weather radar. *Meteorol.l Appl.* **1997**, *4*, 17–21.

(6) Dalili, N.; Edrisy, A.; Carriveau, R. A review of surface engineering issues critical to wind turbine performance. *Renewable Sustainable Energy Rev.* **2009**, *13*, 428–438.

(7) Makkonen, L. Modeling power line icing in freezing precipitation. *Atmos. Res.* **1998**, *46*, 131–142.

(8) Szilder, K.; Lozowski, E. P.; Reuter, G. A Study of Ice Accretion Shape on Cables Under Freezing Rain Conditions. *J. Offshore Mech. Arct. Eng. Trans.* **2002**, *124*, 162–168.

(9) Farzaneh, M., Ed. *Atmospheric icing of power networks*; Springer Science & Business Media, 2008.

(10) Laforte, J.; Allaire, M.; Laflamme, J. State-of-the-art on power line de-icing. *Atmos. Res.* **1998**, *46*, 143–158.

(11) Maitra, T.; Tiwari, M. K.; Antonini, C.; Schoch, P.; Jung, S.; Eberle, P.; Poulikakos, D. On the Nanoengineering of Superhydrophobic and Impalement Resistant Surface Textures below the Freezing Temperature. *Nano Lett.* **2013**, *14*, 172–182.

(12) Maitra, T.; Antonini, C.; Tiwari, M. K.; Mularczyk, A.; Imeri, Z.; Schoch, P.; Poulikakos, D. Supercooled Water Drops Impacting Superhydrophobic Textures. *Langmuir* **2014**, *30*, 10855–10861.

(13) Schremb, M.; Roisman, I. V.; Tropea, C. Different Outcomes after Inclined Impacts of Water Drops on a Cooled Surface. 2015.

(14) Schremb, M.; Roisman, V. I.; Tropea, C. Transient effects in ice nucleation of a water drop impacting onto a cold substrate. *Phys. Rev. E* **2017**, *95*, 022805.

(15) Schremb, M.; Roisman, I. V.; Jakirlić, S.; Tropea, C. Freezing Behavior of Supercooled Water Drops Impacting onto a Cold Surface. 2016.

(16) Hindmarsh, J. P.; Russell, A. B.; Chen, X. D. Experimental and numerical analysis of the temperature transition of a suspended freezing water droplet. *Int. J. Heat Mass Transfer* **2003**, *46*, 1199–1213.

(17) Jung, S.; Tiwari, M. K.; Doan, N. V.; Poulikakos, D. Mechanism of supercooled droplet freezing on surfaces. *Nat. Commun.* **2012**, *3*, 615.

(18) Kong, W.; Liu, H. A theory on the icing evolution of supercooled water near solid substrate. *Int. J. Heat Mass Transfer* **2015**, *91*, 1217–1236.

(19) Schremb, M.; Tropea, C. Solidification of Supercooled Water in the Vicinity of a Solid Wall. *Phys. Rev. E* **2016**, *94*, 052804.

(20) Pruppacher, H. R.; Klett, J. D. *Microphysics of Clouds and Precipitation*, 2nd ed.; Springer, 1997.

(21) Hobbs, P. V. *Ice Physics*; Oxford University Press, 2010.

(22) Reguera, D.; Rubi, J. M. Homogeneous nucleation in inhomogeneous media. II. Nucleation in a shear flow. *J. Chem. Phys.* **2003**, *119*, 9888–9893.

(23) Reguera, D.; Rubi, J. M. Homogeneous nucleation in inhomogeneous media. I. Nucleation in a temperature gradient. *J. Chem. Phys.* **2003**, *119*, 9877–9887.

(24) Ivantsov, G. P. Temperature around a spheroidal, cylindrical and acicular crystal growing in a supercooled melt. *Doklady Akademii Nauk SSSR* **1947**, *58*, 567–569.

(25) Glicksman, M. E.; Schaefer, R. J.; Ayers, J. D. Dendritic growth-A test of theory. *Metall. Trans. A* **1976**, *7*, 1747–1759.

(26) Glicksman, M. E.; Koss, M. B. Dendritic growth velocities in microgravity. *Phys. Rev. Lett.* **1994**, *73*, 573–576.

(27) Shibkov, A.; Golovin, Y.; Zheltov, M.; Korolev, A.; Leonov, A. Morphology diagram of nonequilibrium patterns of ice crystals growing in supercooled water. *Phys. A* **2003**, *319*, 65–79.

(28) Schutzius, T. M.; Jung, S.; Maitra, T.; Eberle, P.; Antonini, C.; Stamatopoulos, C.; Poulikakos, D. Physics of icing and rational design of surfaces with extraordinary icephobicity. *Langmuir* **2015**, *31*, 4807–4821.

(29) Tourkine, P.; Merrer, M. L.; Quéré, D. Delayed freezing on water repellent materials. *Langmuir* **2009**, *25*, 7214–7216.

(30) Jung, S.; Dorrestijn, M.; Raps, D.; Das, A.; Megaridis, C. M.; Poulikakos, D. Are superhydrophobic surfaces best for icephobicity? *Langmuir* **2011**, *27*, 3059–3066.

(31) Boinovich, L.; Emelyanenko, A. M.; Korolev, V. V.; Pashinin, A. S. Effect of Wettability on Sessile Drop Freezing: When Superhydrophobicity Stimulates an Extreme Freezing Delay. *Langmuir* **2014**, *30*, 1659–1668.

(32) Mishchenko, L.; Hatton, B.; Bahadur, V.; Taylor, J. A.; Krupenkin, T.; Aizenberg, J. Design of ice-free nanostructured surfaces based on repulsion of impacting water droplets. *ACS Nano* **2010**, *4*, 7699–7707.

(33) Meuler, A. J.; Mckinley, G. H.; Cohen, R. E. Exploiting Topographical Texture To Impart Icephobicity. *ACS nano* **2010**, *4*, 7048–7052.

(34) Meuler, A. J.; Smith, J. D.; Varanasi, K. K.; Mabry, J. M.; McKinley, G. H.; Cohen, R. E. Relationships between water wettability and ice adhesion. *ACS Appl. Mater. Interfaces* **2010**, *2*, 3100–3110.

(35) Mandal, D. K.; Criscione, A.; Tropea, C.; Amirfazli, A. Shedding of Water Drops from a Surface under Icing Conditions. *Langmuir* **2015**, *31*, 9340–9347.

(36) Lienhard, J. H.; Lienhard, J. H. *A Heat Transfer Textbook*, 3rd ed.; Phlogiston Press: Cambridge, US, 2003.

(37) VDI, *VDI Wärmeatlas*, 10th ed.; Springer Verlag: Berlin, Heidelberg, New York, 2006.

(38) Alexiades, V.; Solomon, A. *Mathematical Modeling of Melting and Freezing Processes*, 1st ed.; Taylor & Francis, 1992.

(39) Baehr, H. D.; Stephan, P. *Wärme- und Stoffübertragung*, 8th ed.; Springer Vieweg: Berlin, Heidelberg, 2013.

(40) Langer, J.; Müller-Krumbhaar, H. Theory of dendritic growth-I. Elements of a stability analysis. *Acta Metall.* **1978**, *26*, 1681–1687.

(41) Langer, J. S.; Müller-Krumbhaar, H. Theory of dendritic growth-II. Instabilities in the limit of vanishing surface tension. *Acta Metall.* **1978**, *26*, 1689–1695.

(42) Müller-Krumbhaar, H.; Langer, J. S. Theory of dendritic growth-III. Effects of surface tension. *Acta Metall.* **1978**, *26*, 1697–1708.

(43) Mullins, W. W.; Sekerka, R. F. Stability of a planar interface during solidification of a dilute binary alloy. *J. Appl. Phys.* **1964**, *35*, 444–451.

Graphical TOC Entry